Electrostatic Sorting of Lunar Regolith Simulants for Sustainable Resource Utilization: Modeling and Characterization of Particle Size Distribution

Abdullah Al Moinee[1]; Peter Bachle[2]; Kyle Newport[3]; William Schonberg[4]; David Bayless[5]; Jeffrey Smith[6]; Daoru Han[7]; and Fateme Rezaei[8]

[1]Linda and Bipin Doshi Dept. of Chemical and Biochemical Engineering, Missouri Univ. of Science and Technology, Rolla, MO. Email: abdullahalmoinee@mst.edu
[2]Dept. of Mechanical and Aerospace Engineering, Missouri Univ. of Science and Technology, Rolla, MO. Email: peter.bachle@mst.edu
[3]Linda and Bipin Doshi Dept. of Chemical and Biochemical Engineering, Missouri Univ. of Science and Technology, Rolla, MO. Email: kant24@mst.edu
[4]Dept. of Civil, Architectural, and Environmental Engineering, Missouri Univ. of Science and Technology, Rolla, MO. Email: wschon@mst.edu
[5]Dept. of Mechanical and Aerospace Engineering, Missouri Univ. of Science and Technology, Rolla, MO. Email: dbayless@mst.edu
[6]Dept. of Materials Science and Engineering, Missouri Univ. of Science and Technology, Rolla, MO. Email: jsmith@mst.edu
[7]Dept. of Mechanical and Aerospace Engineering, Missouri Univ. of Science and Technology, Rolla, MO. Email: handao@mst.edu
[8]Dept. of Chemical, Environmental and Materials Engineering, Univ. of Miami, Miami, FL (corresponding author). ORCID: https://orcid.org/0000-0002-4214-4235.
Email: rezaeif@miami.edu

ABSTRACT

In pursuit of sustainable resource utilization on the Moon, this paper delves into modeling and characterization of particle size distribution (PSD) of lunar regolith simulants in an electrostatic system. A prototype electrostatic sieve was built and tested with four sample simulants mirroring properties of lunar mare and highland regolith. An alternating four-phase (90 degrees, 180 degrees, 270 degrees, 360 degrees) traveling square-wave was utilized for particle-directed transport to model the diverse trajectories of the particles. Numerically, we scrutinized how the distribution functions of the particles are manifested as the electrostatic field propagates, with a focus on three distinct particle ranges (<105, 105–250, 250–500 μm) of four simulants. Results indicated considerable influence of sorting mechanism and control parameters on electrostatic sieve's operation. These parameters encompass column inclination angles (10 degrees, 15 degrees, 20 degrees) and port length (from inlet 10 to 50 cm) at different excitation frequencies (10, 15, 20 Hz) of power source. We optimized parameters in fitting experimental data and successfully identified the movement of particles under electrostatic field at an average feed rate of 0.18 kg/h (0.05 g/s); however, the existing circular system was ineffective and unable to facilitate sorting and separation of the lunar simulant particles. Overall, the results indicate that while our electrostatic sieve instruments are efficient in moving the regolith simulant particles, its design and operation should be further modified for simultaneous transportation and separation of the particles.

Keywords: Lunar regolith, Size distribution modeling, Electrostatic sieve, Extraterrestrial environments, Sustainable resource utilization.

INTRODUCTION

The Moon, Earth's nearest celestial neighbor, has long captured the imagination of scientists, explorers, and space enthusiasts. While historical lunar exploration prioritized scientific research and landing achievements, recent focus has shifted towards potential human presence and lunar habitats. This has underscored the imperative for sustainable resource utilization to support lunar operations and advance space exploration which is essential for reducing the dependency on Earth-supplied resources, significantly cutting mission costs, and ensuring the long-term viability of lunar activities (Symposium on Lunar Bases, 1988; Utilities One, 2023) Unlike Earth, moon lacks a protective atmosphere, exposing it to continuous solar and cosmic radiation, with extreme temperature variations and limited gravity (approximately $1/6^{th}$ that of Earth), posing challenges for lunar operations (Williams 2020; Reitz et al., 2012). In-Situ Resource Utilization (ISRU) addresses challenges by extracting valuable resources from lunar regolith, the layer of loose, fragmented material covering the lunar surface (CSIC Scientific Challenges 2021; Ellery et al., 2017; Moses et al., 2016; Zhang et al., 2023) which is a vast repository of essential materials such as metals, minerals, and volatiles (Anand et al., 2012). Over 50 years, extensive research has laid the foundation for ISRU techniques focused on utilizing lunar regolith[8] for oxygen, water, rocket propellant (Holquist et al., 2021) construction materials (Farries et al., 2021) and energy production (The European Space Agency, 2021; Climent et al., 2014). Scientists simulated lunar surface chemistry, revealing that solar wind protons interacting with lunar electrons generate hydrogen atoms, which in turn, combine with oxygen atoms in the regolith to from hydroxyl ($^{-}$OH), a component of water (H_2O) (Explore, 2019).

Electrostatic sorting leverages the principles of electrostatics to separate lunar regolith particles based on their size and charge properties enhancing the lunar resource extraction process (Adachi, M, Moroka, H, et al., 2017) Developing efficient technologies for resource extraction in the harsh lunar environment is crucial to ensure sustainability and minimize the negative impacts on the lunar environment. Electrostatic sorting efficiently separates and concentrates specific elements or compounds in lunar regolith, allowing targeted extraction (Sanders et al., 2005) based on their charge and size (Adachi et al., 2017) and can obtain specific size fractions, gravity (Kawamoto, et al., 2022) and purity levels (sang, et al., 2023) optimizing ISRU processes. Compared to traditional non-electrostatic mechanical and chemical separation methods, electrostatic sorting can be more cost/energy-efficient nature, with fewer moving parts and lower consumable requirements, makes electrostatic sorting an attractive for lunar resource utilization The lunar regolith's fine particle size (<20 μm) poses challenges to standard mineral processing; addressing this issue, methods like vibrating classifiers, electrostatic travelling waves could remove large particles and enable beneficiation and metal reduction processes with slightly larger feed material sizes in low gravity, static-charging lunar conditions (Sanders, et al., 2005; Artemis III Science, 2020; Matthew et al., 2022). In the high vacuum and low gravity of outer space, external forces, particularly the electric force, are essential for particle transport. The electrostatic method first proposed in 1967, demonstrating that electrostatically charged particles in the sorting system experience dielectrophoretic and Coulomb forces in an alternating non-uniform electrostatic field, countering reduced gravity and adhesion effects for particle movement and transport (Gu et al., 2021). Mastering the process of electrostatic lunar regolith beneficiation can have a broader implication across the solar system, including asteroids and Mars addressing similar challenges and opportunities.

SIMULANTS AND EXPERIMENTAL SETUP

Description of sample simulants. In order to facilitate experiments and simulations relevant to lunar surface technology, the utilization of lunar regolith simulants has become indispensable mimicking lunar surface properties. The chosen simulants from Off Planet Resources (OPR), LLC, a collaborative partner in the project, were selected to encompass a broad spectrum of potential lunar surface conditions which are categorized based on composition and particle size. Composition variations include primary rock type, agglutinate concentration, and iron additives, while size distributions are classified as coarse, medium, and fine. The rock composition comprises feldspar-rich (70% to 90%) highland type and feldspar-poor (65% to 50%) mare type. Highland simulants consist of 90% anorthosite and 10% basalt before agglutinate addition, while mare simulants comprise 90% basalt and 10% anorthosite before agglutinate addition. Agglutinates, representing glass-trapped minerals similar to nano-breccias, are added after establishing rock percentages. We aimed at sorting regolith simulants based on their particle size, and assessing how their separation is affected by their motion and mobility in electrostatic sieving device. Our simulated lunar regolith comprises particle of varying sizes, with specific attention given to those in the submicron and micrometer ranges, reflective of the dominant constituents of lunar regolith. This investigation employs four unique regolith simulants, presented in **Table 1**, to highlight their fidelity as precise models for lunar soil properties.

Table 1. Composition of Sample Simulants.

Simulant	Composition			Lunar Region	Particle Size Classification		
	Anorthite %	Agglutinates %	Basaltic Minerals %		<105 µm	105-250 µm	250-500 µm
L2W10g6	10	10	90	Mare	☑	☑	☑
L2W60g6	10	60	90	Mare	☑	☑	☑
H4W10g6	90	10	10	Highland	☑	☑	☑
H4W60g6	90	60	10	Highland	☑	☑	☑

When a sample is labelled as L2W10g814s1 or H4W60g6s5, L2W10 or H4W60 denotes OPR designations, L2, H4 denote rock type (mare or highland); W10, W60 denote agglutinate percentage (10 % or 60%); g6 denotes Mesh #60, 500 to 250 microns and g814 denotes Mesh #80 to 140, 250 to 105 microns, and s1 or s5 denotes the slot number for the distributed particles. These samples were prepared under controlled laboratory conditions to ensure homogeneity and minimize potential agglomeration of particles.

Design of experimental setup. We developed and characterized a prototype electrostatic sieve system, crucial for understanding particle size distribution (PSD). The custom-designed electrostatic sieve separator, tailored for lunar regolith processing, utilizes electrostatic properties to separate particles based on size. While sieving and electro-magnetic separation are well-established in ore processing, the lunar environment lacks the luxury of fluids and significant gravity. To adapt sieving to the extreme lunar conditions, electrostatics must replace fluids. All electrostatic sieve prototypes necessitated electronic components for operation, including a pair of FY6600-60M waveform generators, a 12-Volt, 2-Amp DC power source for the amplifier, which generated a 2-3 kV signal at 0.002-0.003 Amps. A four-phase traveling

square wave (oscilloscope) was employed to verify the signal transmitted through the electrostatic sieve which were chosen for its clear signal transitions that facilitates precise control over particle trajectories with simplicity, controllability, and effectiveness in inducing electrostatic forces. The wave's amplitude and frequency were carefully calibrated following the insights gained from prior research, to ensure precise control over particle trajectories (Adachi, M, Hamazawa, K, et al., 2017; Adachi, M, Moroka, H, et al., 2017; Anand, et al., 2012). The supporting equipment configuration and schematic are depicted in **Figure 1**.

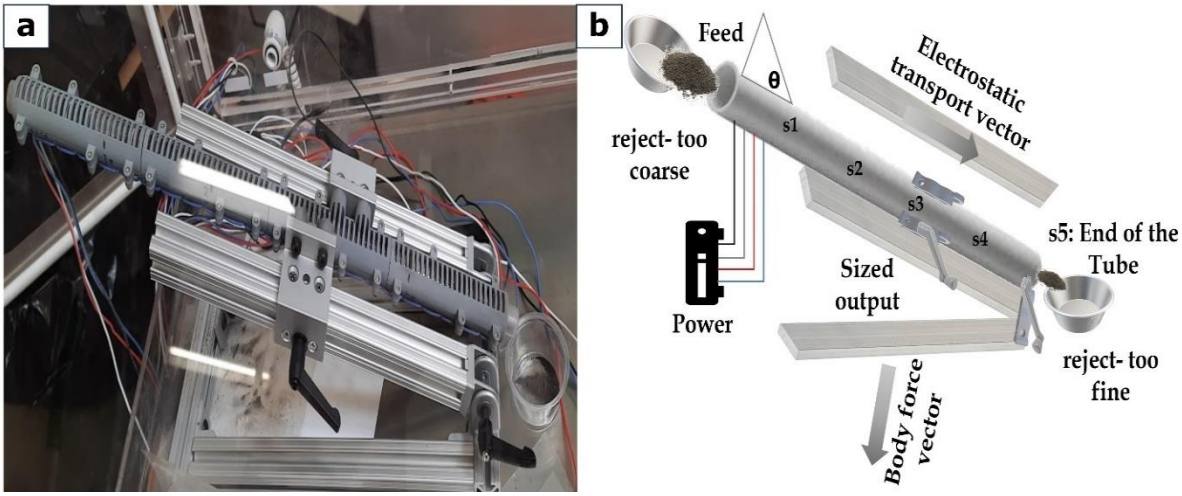

Figure 1. (a) Experimental setup of electrostatic sieving system, and (b) schematic of the prototype; s stands for slot number.

MODELING

Numerical calculations for PSD. Our electrostatic traveling wave system utilizes alternating voltages and embedded electrodes to transport charged particles through triboelectricity. Employing a numerical model, we discretized particle distribution into size bins, tracking motion under evolving Coulomb and dielectrophoretic forces. This MATLAB-based model offers real-time, high-fidelity simulations, calibrated rigorously against experimental data. Assuming particle distribution is influenced by a separator's electrostatic force, modeled as sinusoidal variation for the transportation, flow pattern, and kinetics with varying angles and frequencies, our system optimizes particle sorting dynamics. A static time-stepping interaction model was assumed to simulate the behavior of charged particles considering their charge states and positions within the sieve to track the motion of over time. To ensure the accuracy and reliability of our simulation model, it underwent rigorous calibration and validation against data obtained from experiments. The **equation (1)** presented is an empirical model describing the sinusoidal variation in PSD. We assumed for our model that the PSD, $P(\phi)$ at a particular phase angle (ϕ) is influenced by the separator angle (α) and frequency (f):

$$\mathbf{P(\phi,\alpha,f) = A(\alpha)\cdot\sin(f\cdot\phi + \phi_0) + B(\alpha)} \quad \mathbf{(1)}$$

where $A(\alpha)$ and $B(\alpha)$ in the equation represent amplitude and baseline distribution, respectively, influenced by the inclination. ϕ_0 is a phase shift parameter that might capture any

phase offset in the distribution. The frequency of the separator's rotation affects the rate at which this variation occurs (Gorshenin, et al. 2020) This the equation can characterize the parameters influencing PSD, P(ϕ,α,f), representing kinetics or fluid-related characteristics, with implied boundary conditions.

The Microtrac S3500, underwent particle size analyses, running each sample four times with volume-reflecting, volume-absorbing, count-reflecting, and count-absorbing parameters. In this regard, multimodal particle density function (PDF) can be expressed as a weighted sum of individual PDF where each mode represents a distinct peak in the particle distribution,

$$\mathbf{P(d)} = \sum_{\mathbf{i}=1}^{\mathbf{N}} \mathbf{wi} \ \frac{1}{\sigma\sqrt{2\pi}} \ e^{-\frac{\left(x-\mu i\right)^2}{2\sigma \mathbf{i}^2}} \quad \textbf{(2)}$$

where, P(d) is the PDF function in **equation (2)**, N is the number of modes (peaks) in the distribution, w_i are the weights associated with each mode, indicating the contribution of each mode to the overall distribution, μ_i represents the mean (center) of the i^{th} mode, σ_i is the standard deviation of the i^{th} mode, controlling the width of the mode, e is the base of the natural logarithm. Each mode is essentially a log-normal Gaussian distribution, and the weighted sum combines these modes to form a multimodal PDF. We also consider,

$$\mathbf{S(p,d) = y(p,d)} \quad \textbf{(3)}$$

where S(p,d) represents the size distribution (in percentage) of particles at position d for a given particle size p in **equation (3)** and p represents the index of particle size categories (e.g., 1 for '<105 μm', 2 for '105-250 μm', and 3 for '250-500 μm').

Along the sieve slit distance, we employed a logistic function to model the mechanism of this phenomena in the percentage of particles separated through the sieve. The logistic function, represented as

$$\mathbf{F(x)} = \frac{L}{1+e^{-k(x-x0)}} \quad \textbf{(4)}$$

where F(x) is the percentage separated at distance x, L is the maximum percentage separated, k is the logistic growth rate, and x_0 is the distance at which F(x) is halfway between the minimum and maximum, proved to be a suitable choice for capturing the sigmoidal behavior exhibited by the data as shown in **equation (4)**. The logistic growth rate can be interpreted as the rate at which the percentage separated changes concerning the distance along the sieve slit. It influences how quickly the separation process approaches its maximum percentage. The code utilized this logistic function to fit the experimental data and create a comprehensive figure depicting the mass percent separated per slit along the electrostatic sieve in varying inclination and mesh number.

RESULTS AND DISCUSSIONS

Slot-wise Particle Size Distributions. Analyzing PSD for four lunar regolith samples (H4W60g6, L2W60g6, H4W10g6, L2W10g6) offers insights into regolith characteristics essential for efficient resource utilization and exploration on lunar surface within the three-size

range. **Figure 2** illustrates a predominant presence of particles in the "250-500 μm" range, followed by the "105-250 μm" range, with particles smaller than 105 μm being the least abundant. This distribution aligns with expected lunar regolith characteristics shaped by geological forces, impact events, and the lunar environment. The delineation of particle size distribution informs the design of machinery for resource exploitation. Larger impacts contribute to particles in the "250-500 μm" range, while smaller impacts produce finer particles in the "105-250 μm" range, easily transported and accumulated. The dominance of the "250-500 μm" range suggests a balance in processes transporting and accumulating regolith particles. The Moon's lower gravity allows unique sedimentation, where smaller particles may remain suspended, contributing to the prevalence of finer particles (Beale 2007).

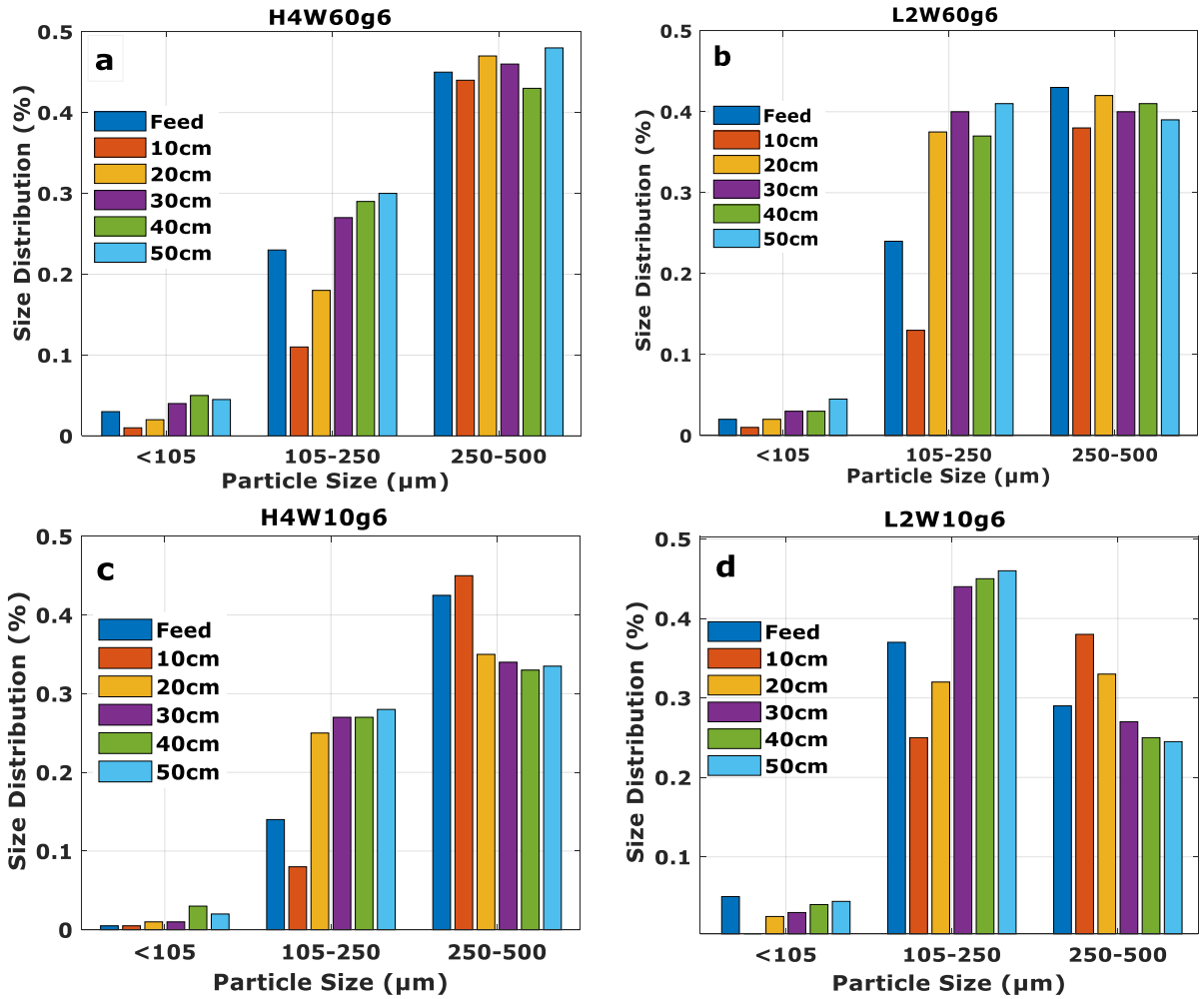

Figure 2. Experimental PSD profiles of lunar regolith samples (a) H4W60g6, (b) L2W60g6, (c) H4W10g6, and (d) L2W10g6.

Figure 3 depicts the slot-wise distribution percentage of four lunar simulants across the six slots of the sieve system: feed slot (inlet), slot1 was located at 10 cm, slot 2 at 20 cm, slot 13 at 30 cm, slot 4 at 40 cm, and end slot (outlet) was located at 50 cm from the inlet slot for the feed.

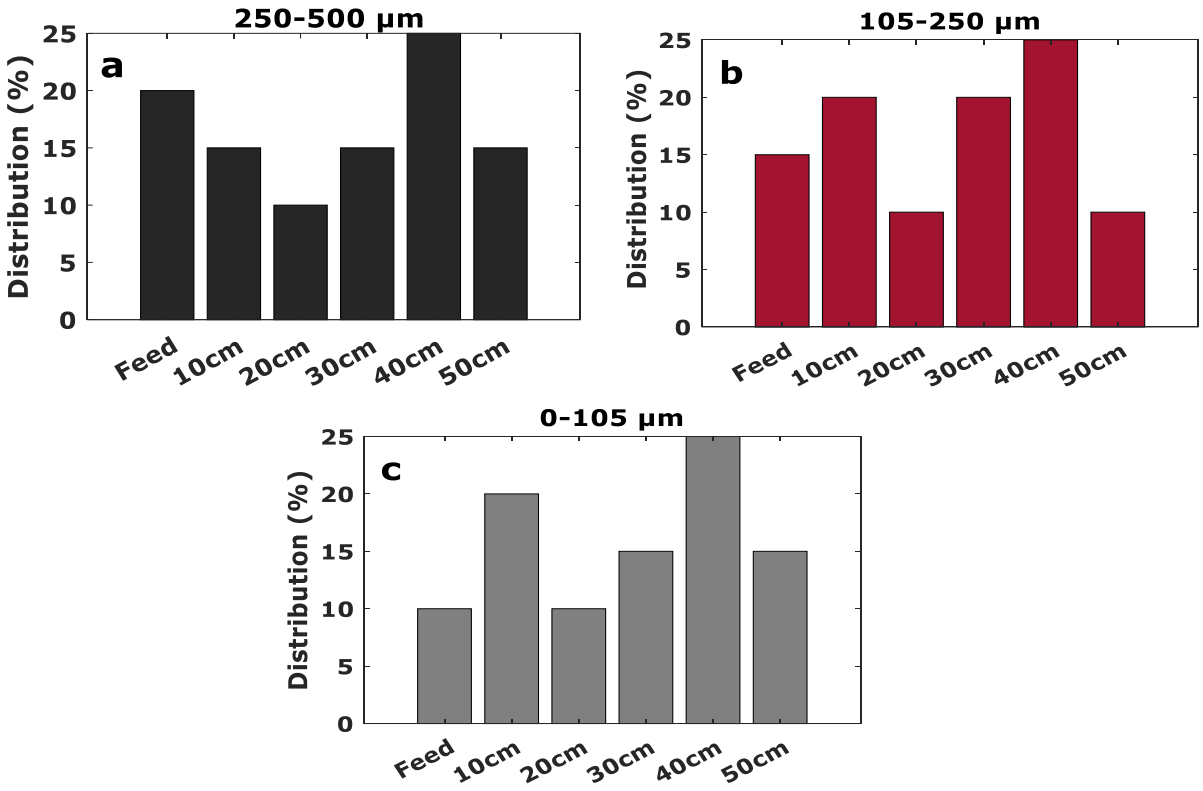

Figure 3. Slot-wise distribution percentage of 4 lunar simulants for 3 classified ranges: (a) 250-500 µm, (b) 105-250 µm, and (c) 0-105 µm.

The analysis, utilizing modeling assumptions and equations, reveals a concentration of simulants in slot4, presented higher distribution percentage signifying the concentration of simulants within that specific region intricating the transportation under electrostatic force without sorting since the particles were moving equally well at the specific frequencies.

Validation of Experimental Data and Model Validation. In this section, we aimed at analyzing the PSD and PDF of lunar regolith samples under various experimental setups. The PDF enriches our understanding by quantifying the likelihood of encountering particles of different sizes. The following graphs depict the modeled PSD and PDF for each experimental condition aiming at a comparative approach. Minor discrepancies may arise from factors like measurement errors and variations in experimental conditions. The similarity in shapes between experimental and model distributions, as shown in **Figure 4**, underscores the reliability of our methodologies and model assumptions. The agreement between experimentally observed PDF and model-based PDF supports the validity of the log-normal distribution model, although real-world complexities and experimental factors may introduce deviations.

Figure 4(a)-4(f) shows the remarkable consistency between the experimental and model data trends for simulant H4W10g6 and H4W60g6 respectively particularly in their shape, peak and trough alignment, and continuous behavior, which has far-reaching consequences for the efficiency and reliability of the electrostatic sieve modeling system. The alignment of peaks and troughs between experimental and model trends indicates the model's efficacy in predicting the regions within the specified particle size range where particle density is highest and lowest. The

predictive ability is crucial for optimizing the electrostatic sieve system, enabling efficient particle transport and separation.

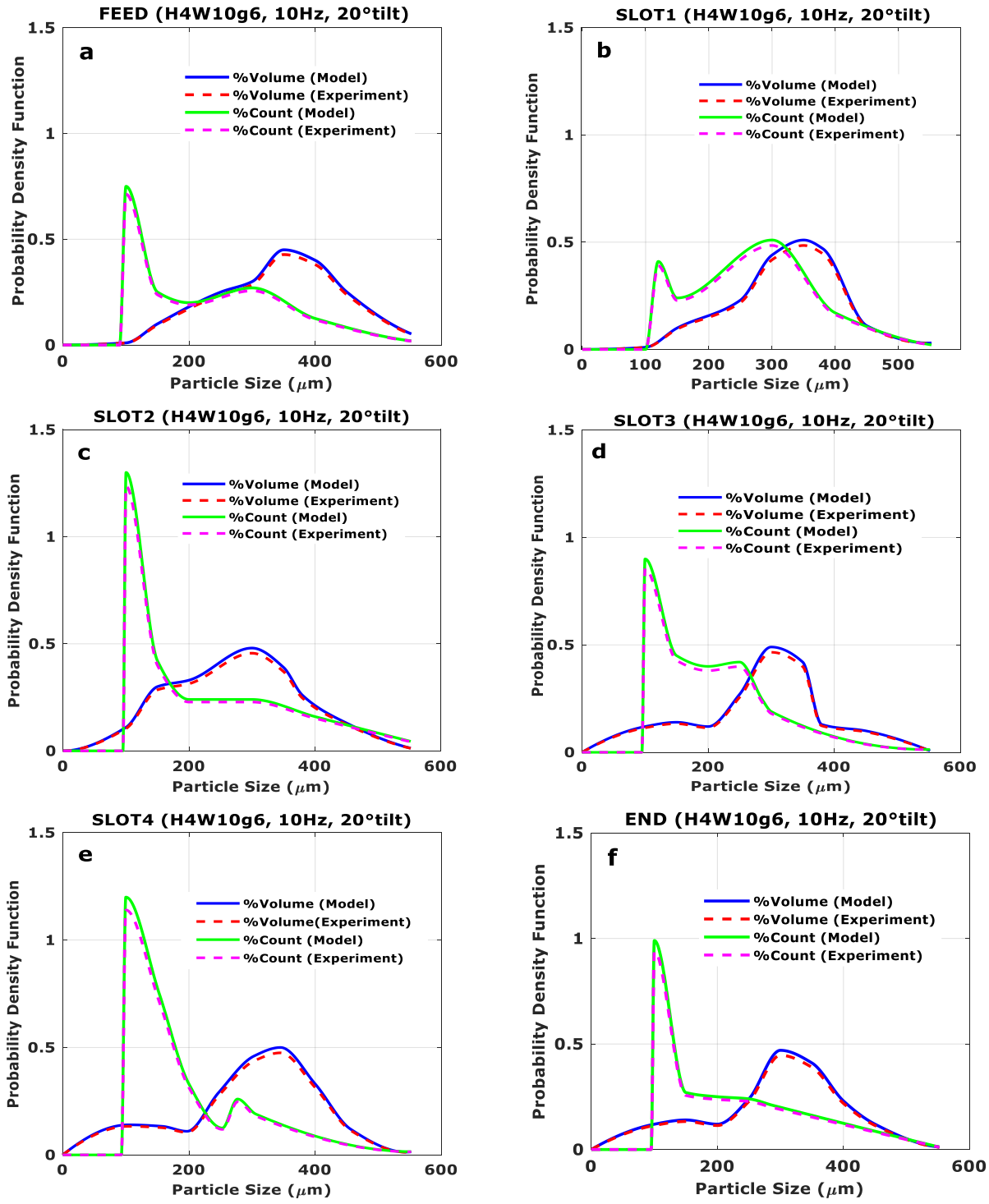

Figure 4. PDF profiles for H4W10g6 across (a) feed, (b) slot 1, (c), slot 2 (d), slot 3, (e), slot 4, and (f) end slots of electrostatic system at 10 Hz and 20° tilt.

The model's ability to consistently reproduce the observed particle size distribution trends demonstrates its precision in predicting particle behavior. the "count" parameters yielded unreliable data, while the "volume" parameters demonstrated reliability when compared to known sample particle size distributions. It is clear from **Figure 4a to Figure 4f** that for H4W10g6, PDF exceeds 1 at slot2 for count in the particle size analyzer which indicates the particle between 0-200 µm are densely located there which is larger than a uniform distribution. In case of other slots for H4W10g6, it is clear that more than two slots provided the dense population of particles from slot2 to slot4 within a uniform range between 0-50 µm. In the generated plots, we observe that both the experimental and model trends exhibit similar patterns, with characteristic peaks and valleys. This simulant followed the same patterns but with different concentrations during transport at different slot specifically from slot2-4 corresponding to the evident multimodal depiction of the PDF validated by **equation (2)**.

When closely examining the plots, we notice that the peaks and troughs in the experimental and model trends often coincide with a uniform distribution supporting the transport of the particles without sorting for L2W10g6 and L2W60g6. This alignment indicates that the model accurately predicts the positions where particle density is highest (peaks) and lowest (troughs) within the given size range. For example, S10 and S15 shows that slot3 and slot2 for L2W10g6 and L2W60g6 respectively provided a denser population of particles from 0-200 µm a smaller population of particles from 200-400 µm. On the other hand, S9 and S17 shows that slot2 and slot4 for L2W10g6 and L2W60g6 respectively provided a denser population of particles from 0-150 µm a smaller population of particles from 150-250 µm. Continuous nature of trends is a significant aspect of validation, indicating that both data sources represent a coherent and connected distribution of modeled particle sizes. Our lunar regolith simulants exhibit a multimodal particle size distribution, which is consistent with the lunar surface. This distribution comprises a dominant fraction of submicron-sized particles, a secondary fraction in the micron range, and a minor fraction of millimeter-sized particles. The presence of submicron particles is of particular interest due to its relevance in dust-related lunar surface challenges (Colwell, et al., 2007). he majority of particles fall within the fine fraction (submicron to micron range), comprising a significant percentage of the total mass. While the majority of particles are in the fine fraction, a notable tail of coarse particles extends into the millimeter range. These larger particles are significant for engineering aspects such as excavation, drilling, and mobility, where particle size directly influences equipment design and performance (Ruess et al., 2006).

Sensitivity of Transport Control Parameters. The angles tested were 10°, 15°, and 20°, while the frequencies at power source used were 10, 15, and 20 Hz for the three size ranges of the particles. Analyzing the model's sensitivity to phase angle, inclination, and electrical frequency, as depicted in the obtained PSD plots (**Figure 5**), provides valuable insights into the behavior of lunar regolith via particle size distribution within the inclined electrostatic separator. It is evident from these plots that the angle of inclination significantly affects the PSD profiles for all four simulants. As the angle increases from 10° to 20°, notable variations in the distribution pattern can be observed, clearly implying that the angle plays a crucial role in the motion and separation of the electrostatic separator, as validated by **equation (1)**. The plots also reveal the impact of frequency on the PSD profiles. Different frequencies result in distinct distribution patterns, indicating that the frequency of the applied square wave current affects the process. Higher frequencies might promote finer particle separation, while lower frequencies may favor the motion of coarser particles be separated. The particle size range also influences the distribution pattern. For instance, particles in the range of 250-500 µm exhibit a different distribution trend compared

to particles in the range of 105-250 µm or those smaller than 105 µm. This suggests that the electrostatic separator might exhibit varying efficiency for different particle size ranges under applied electromotive and dielectrophoretic force. The plots provide a visual representation of the PSD in the inclined electrostatic separator for different angles, frequencies, and particle size ranges. These results serve as a basis for further analysis and can guide future experimental investigations to optimize the separation process for lunar regolith particles.

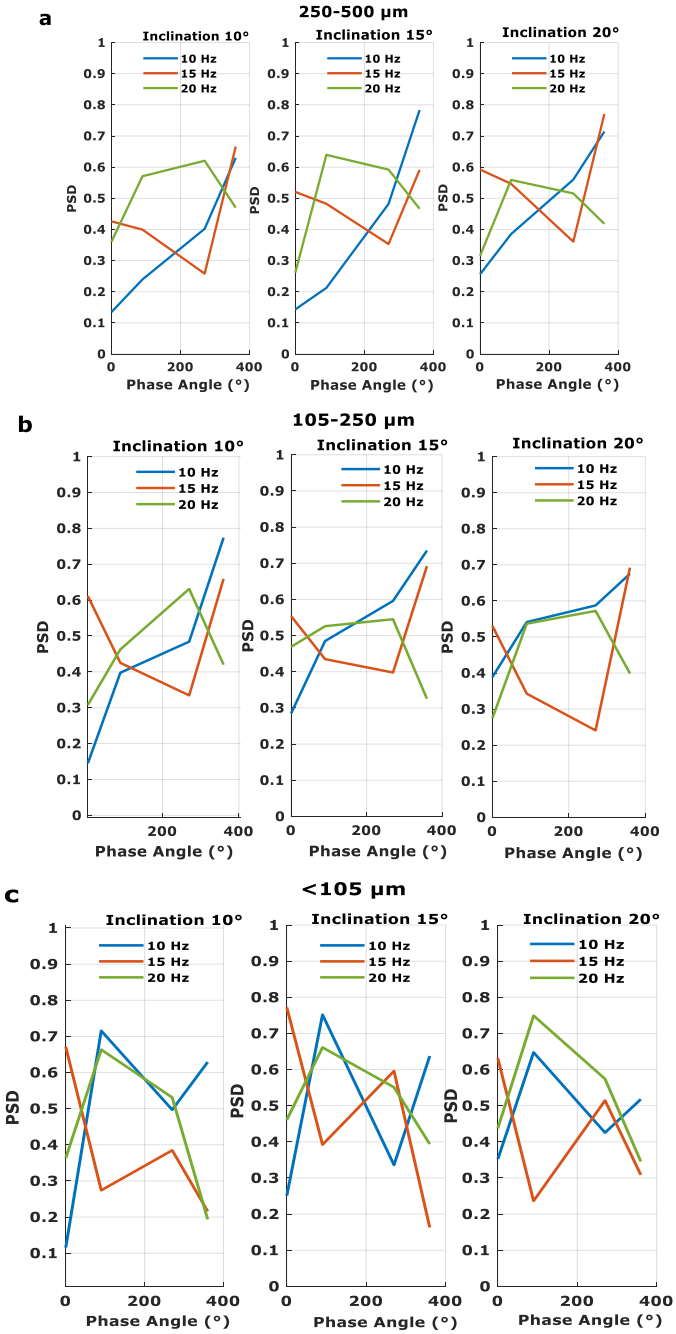

Figure 5. Variations in phase angles with PSD for specified inclinations and excitation frequencies at (a) 250-500 µm, (b) 105-250 µm, and (c) 0-105 µm size ranges.

Phase angle determines the timing and direction of the electrostatic forces acting on lunar regolith particles within the separator. By manipulating this independent variable, we can systematically investigate its influence on the PSD under specific inclinations and frequencies. Varying the phase angle allows us to assess how particles respond to changing electrostatic forces, helping us optimize the separation process. **Figure 6** reflects the mechanism of the phenomena by the logistic function model of **equation (4)**. The significance of mesh number and inclination affect the particle transport and separation efficiency, influencing the shape and steepness of the curves, rate and extent of material passing through sieve for 4 types of lunar regolith simulants. Figure 6 depicted that the increasing inclination resulted in increasing percent of total mass through sieve and increasing mesh number resulted in decreasing percentage.

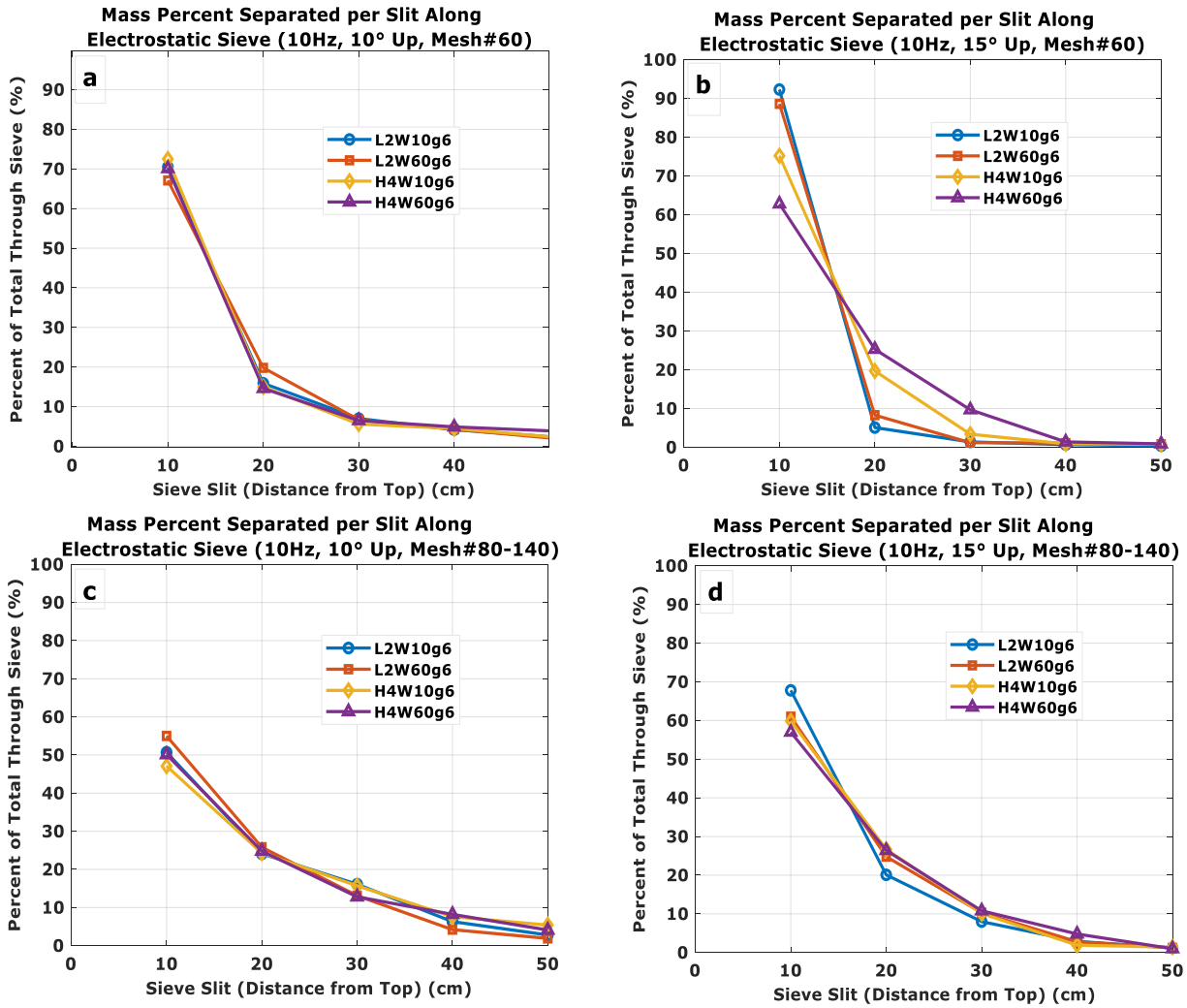

Figure 6. Mass percent separated per slit along the electrostatic sieve at 10 Hz and different frequency and mesh number/type with an approximate feed rate of 0.18 kg/h: (a) 10° tilt, Mesh#60, (b) 15° tilt, Mesh#60, (c) 10° tilt, Mesh#80-140, and (d) 15° tilt, Mesh#80-140.

Model Prediction and Decision. The utilization of the 4-phase electrostatic sieve tube represents a significant breakthrough in the domain of particle manipulation, particularly within the size range of 100-500 μm. This innovative technology has demonstrated remarkable efficacy

in the transportation of particles falling within this size spectrum, with a capacity ranging from 0.04 to 0.06 g/s (equivalent to 0.15 to 0.22 kg/h). To fully comprehend the capabilities of this apparatus, it is essential to delve into the underlying principles and parameters that govern its operation. One of the pivotal factors influencing the success of the electrostatic sieve tube is the inclination of the terrain. It has been established that optimal performance is achieved when the slope of descent remains less than the angle of repose, which is approximately 10° to 20°. Furthermore, the electrostatic sieve tube showcases its prowess by effectively navigating ascending slopes of up to 20° under the influence of terrestrial gravity (**Figure 7a**). This ability to operate on diverse terrain is a testament to the versatility and adaptability of this technology.

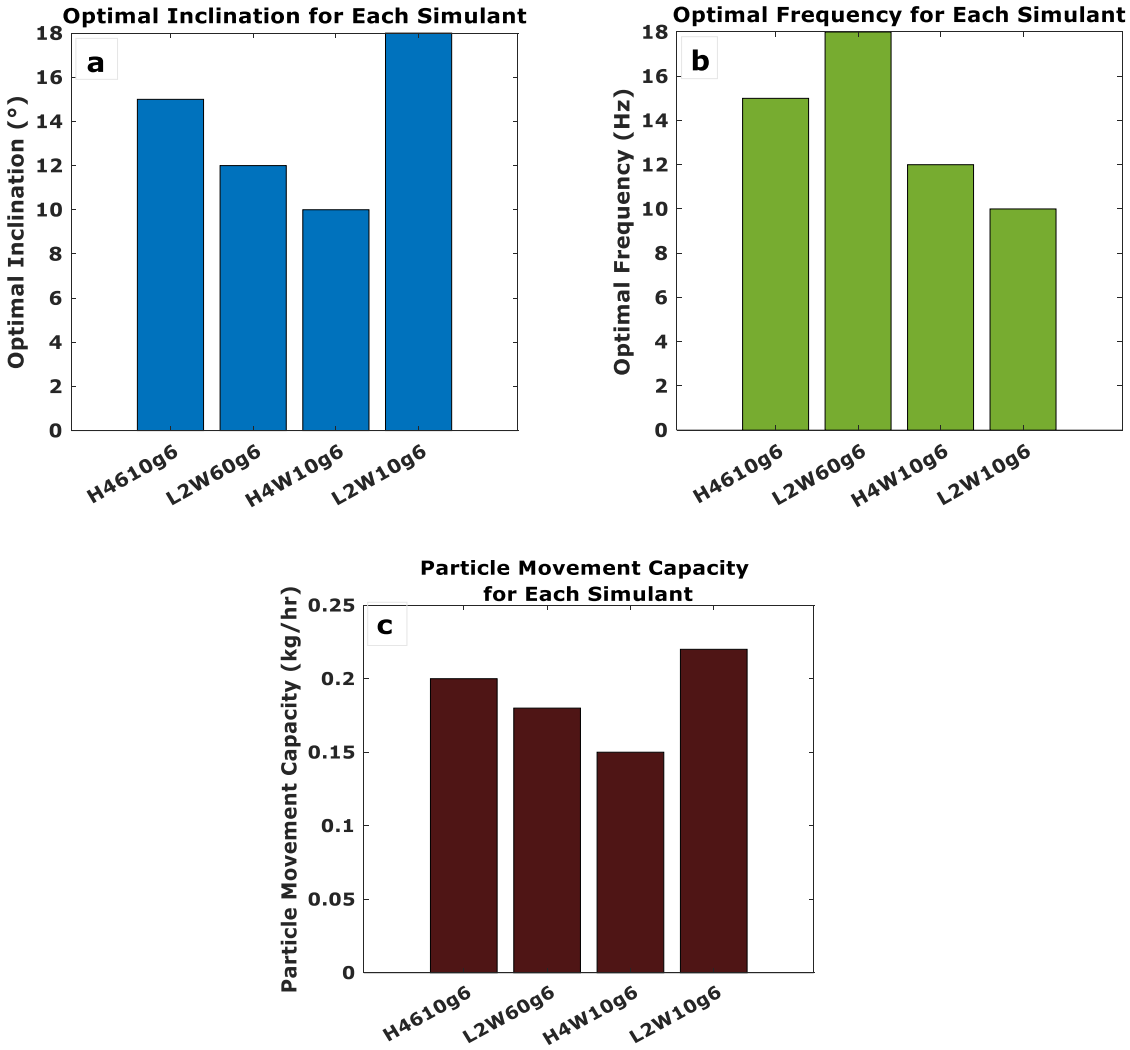

Figure 7. Prediction for simulant-specific (a) optimal inclination, (b) optimal frequency, and (c) particle movement capacity.

Intriguingly, the performance of the electrostatic sieve tube is not uniform across all frequencies. Through meticulous experimentation and modeling approach, it has been predicted that signal frequencies ranging from 7 Hz to 20 Hz yield the most favorable results (**Figure 7b**). Within this frequency range, the particle movement is not only maximized but also exhibits a

degree of precision and control (**Figure 7c**). However, it is noteworthy that as one ventures beyond this optimal frequency range, the efficiency of particle movement diminishes progressively. These characteristic warrants careful consideration in the practical implementation of the electrostatic sieve tube efficiently.

Our system is modeled specifically for lunar regolith sorting comparing other sorting system without the consideration of extraterrestrial environment and the proposed system was geared for transportation of the simulants for lunar environment and the system operates effectively in a vacuum condition, eliminating the need for gases, liquids, or complex mechanical components, simplifying the operational setup and maintenance. While existing sorting systems showed effective sorting particles smaller than 20 μm,[15] our model offers the added advantages of scalable adaptability for particles of various sizes including those above 20 μm. Dwari et al., (2009) investigated the tribo-charging of solids focusing on charge acquisitions during tribo-electrification where they originally remain uncharged till they came into contact and our system was designed on supplied electrostatic field propagating on charge acquisition in particles to set them into motion. Besides, the model utilized an innovative alternating four-phase traveling square-wave for particle-directed transport, allowing for diverse particle modeling and control comparing the recent investigations on particle transport on moon using alternating current (Gu et al., 2022). Moreover, the proposed sorting system excels in particle behavior analysis by providing more meticulous examination of various aspects, including changes in velocity vector distribution induced by the electrostatic field observing the patterns of velocity under fixed excitation frequency and column inclination. Thus, the model uniquely offers valuable insights into frequency-dependent sorting for future ventures. Notably, our system can achieve backward particle transport as well under specific conditions, opening up the possibility of unique applications in lunar regolith processing. Most importantly, this proposed system and model employs comprehensive analysis utilizing the unique features of setup and distinct element method to replicate experimental results and predict system performance simultaneously in lunar environment optimizing the critical control parameters. Yet, a significant limitation of this technology becomes evident upon closer examination. While it excels in particle transportation, it does not possess the capability to sort or sieve particles based on size or other attributes. This limitation arises from the fact that all particles respond equally well to the specific frequencies employed by the electrostatic sieve tube. Consequently, the technology is more aptly described as a conveyance mechanism rather than a sieve in the traditional sense.

CONCLUSION

The exploration of space, particularly the Moon, presents humanity with unprecedented challenges and opportunities. Among these challenges, the efficient and sustainable utilization of lunar resources stands as a critical necessity for prolonged space exploration and eventual habitation. In this pursuit, modeling emerges as a linchpin upon which our understanding of lunar regolith behavior and resource extraction processes is built with an innovative approach of electrostatic sieve system. The system's effectiveness on diverse terrains, optimized performance at specific frequencies, and efficient particle transportation capacity makes it a noteworthy innovation in the field where the sorting effectiveness can be achieved by incorporating variable frequencies and implementing advanced real-time feedback control algorithms. Accurate numerical representations of complex physical phenomena unlock profound insights into particle and material behavior in low-gravity environments which may be

adjusted via electric field strength concerning affected particle motion and dynamics of electrostatic separation. The validation and agreement in trend shape and continuous behavior between the model and experimental data underscores the reliability of the model in representing the physical processes governing particle distribution in lunar regolith. This reliability instills confidence in the electrostatic sieve system's performance under various lunar surface conditions. Engineers can have greater assurance that the system will function as intended, even in the presence of uncertainties. Scaling up the sorting rate involves optimizing hardware, increasing sorting slots, refining waveform characteristics, and exploring parallel processing approaches or multiple electrostatic sieve systems for higher throughput. However, the inability to sort or separate between particles based on size or other characteristics underscores the need for a nuanced approach when considering its applications. Further research and development efforts to construct a potentially modified setup that works finely both for separation and transportation which may yield insights into complementary technologies to harness the full potential of this novel electrostatic sieve system. Ongoing efforts aim to bridge the gap in our setup by developing a comprehensive system capable of both monitoring particle motion and predicting effective separation. This underscores modeling's paramount importance in shaping sustainable resource utilization strategies on the Moon and beyond, with profound implications for space exploration and resource exploitation methodologies.

REFERENCES

Adachi, M., Moroka, H., Kawamoto, H., Wakabayashi, S., and Hoshino. T. (2017). "Particle-Size Sorting System of Lunar Regolith Using Electrostatic Traveling Wave." *Journal of Electrostatics* 89: 69–76. https://doi.org/10.1016/j.elstat.2017.08.002.

Adachi, M., Hamazawa, K., Mimuro, Y., and Kawamoto, H. (2017). "Vibration Transport System for Lunar and Martian Regolith Using Dielectric Elastomer Actuator." *Journal of Electrostatics* 89: 88–98. https://doi.org/10.1016/j.elstat.2017.08.003.

Anand, M., Crawford, I. A., Balat-Pichelin, M., Abanades, S., Westrenen, W. van, Péraudeau, G., Jaumann, R., and Seboldt. W. (2012). "A Brief Review of Chemical and Mineralogical Resources on the Moon and Likely Initial In Situ Resource Utilization (ISRU) Applications." *Planetary and Space Science* 74 (1): 42–48. https://doi.org/10.1016/j.pss.2012.08.012.

Artemis III Science Team Definition Report (NASA/SP-20205009602188). (2020). *A Bold New Era of Human Discovery*. https://www.nasa.gov/wp-content/uploads/2015/01/artemis-iii-science-definition-report-12042020c.pdf

Beale, D. The Lunar Environment and Issues for Engineering Design (Chapter 5). Fundamentals of Lunar and Systems Engineering. https://www.eng.auburn.edu/~dbeale/ESMDCourse/Chapter5.htm

Climent, B., Torroba, O., González-Cinca, R., Ramachandran, N., and Griffin, M. D. (2014). "Heat Storage and Electricity Generation in the Moon during the Lunar Night." *Acta Astronautica* 93: 352–58. https://doi.org/10.1016/j.actaastro.2013.07.024.

Colwell, J. E., Batiste, S., Horányi, M., Robertson, S., and Sture, S. (2007). "Lunar Surface: Dust Dynamics and Regolith Mechanics." *Reviews of Geophysics* 45 (2): 1–26. https://doi.org/10.1029/2005RG000184.

CSIC Scientific Challenges: Towards 2030. (2021). *In-Situ Resources Utilization*, 12, 13–41. https://digital.csic.es/bitstream/10261/259692/1/In-situ%20resource%20utilization_LIBRO%20BLANCO%20CSIC%2012.pdf

Dwari, R. K., Rao, K. H., and Somasundaran, P. (2009). "Characterisation of Particle Tribo-Charging and Electron Transfer with Reference to Electrostatic Dry Coal Cleaning." *International Journal of Mineral Processing* 91 (3): 100–110. https://doi.org/10.1016/j.minpro.2009.02.006.

Ellery, A., Lowing, P., Wanjara, P., Kirby, M., Mellor, I., and Doughty, G. (2017). "FFC Cambridge Process with Metal 3D Printing as Universal In-Situ Resource Utilisation." *14th Symposium on Advanced Space Technologies in Robotics and Automation (ASTRA)*, no. June: 20–22. https://robotics.estec.esa.int/ASTRA/Astra2017/1.%20Wednesday%2021%20June/6A%20Extraterrestrial%20Sampling%20II/6A_16.20_Ellery.pdf

Explore. (2019). *NASA Scientists Show How Ingredients for Water Could Be Made on Surface of Moon, a 'Chemical Factory'*. https://www.nasa.gov/missions/nasa-scientists-show-how-ingredients-for-water-could-be-made-on-surface-of-moon-a-chemical-factory

Farries, K. W., Visintin, P., Smith, S. T., and Eyk, van P. (2021). "Sintered or Melted Regolith for Lunar Construction: State-of-the-Art Review and Future Research Directions." *Construction and Building Materials* 296: 123627. https://doi.org/10.1016/j.conbuildmat.2021.123627.

Gorshenin, A., Korolev, V., and Zeifman, A. (2020). "Modeling Particle Size Distribution in Lunar Regolith via a Central Limit Theorem for Random Sums." *Mathematics* 8 (9): 1–24. https://doi.org/10.3390/MATH8091409.

Gu, J., Zhang, G., Wang, Q., Wang, C., Liu, Y., Yao, W., and Lyu, J. (2022). "Experimental Study on Particles Directed Transport by an Alternating Travelling-Wave Electrostatic Field." *Powder Technology* 397: 117107. https://doi.org/10.1016/j.powtec.2022.117107.

Gu, J., Wang, Q., Wu, Y., Lele, F., Zhang, G., Li, S., Tian, L., and Yao, W. (2021). "Numerical Study of Particle Transport by an Alternating Travelling-Wave Electrostatic Field." *Acta Astronautica* 188: 505–17. https://doi.org/10.1016/j.actaastro.2021.07.043.

Holquist, J. B., Gellenbeck, S., Bower, C. E., and Tewes, P. (2021). "Experimental Proof of Concept of a Cold Trap as a Purification Step for Lunar Water Processing." *50th International Conference on Environmental Systems*, 292, 1-14. Available at: https://ttu-ir.tdl.org/bitstreams/3431727b-5363-49b9-9e3e-587a172d4a61/download

Kawamoto, H., Morooka, H., and Nozaki, H. (2022). "Improved Electrodynamic Particle-Size Sorting System for Lunar Regolith." *Journal of Aerospace Engineering* 35 (1): 1–7. https://doi.org/10.1061/(asce)as.1943-5525.0001371.

Matthew, S., Matthew, H., Geoffrey, B., Rhamdhani, A., Duffy, A., and Pownceby, M. (2022). "Mineral Processing and Metal Extraction on the Lunar Surface — Challenges and Opportunities." *Mineral Processing and Extractive Metallurgy Review* 43 (7): 865–91. https://doi.org/10.1080/08827508.2021.1969390.

Moses, R. W., and Dennis, M. B. (2016). "Frontier In-Situ Resource Utilization for Enabling Sustained Human Presence on Mars." *NASA Scientific and Technical Information*, no. April 2016. https://ntrs.nasa.gov/search.jsp?R=20160005963%0Ahttps://ntrs.nasa.gov/archive/nasa/casi.ntrs.nasa.gov/20160005963.pdf.

Guenther, R., Berger, T., and Matthiae, D. (2012). "Radiation Exposure in the Moon Environment." *Planetary and Space Science* 74 (1): 78–83. https://doi.org/10.1016/j.pss.2012.07.014.

Ruess, F., Schänzlin, J., and Benaroya, H. (2006). "Structural Design of a Lunar Habitat." *Journal of Aerospace Engineering* 19 (3): 133–57. https://doi.org/10.1061/(asce)0893-1321(2006)19:3(133).

Sanders, G. B. and Duke, M. (2005). "In-Situ Resource Utilization (ISRU) Capability Roadmap Progress Review." *Capabilities Roadmap Briefings to the National Research Council*. https://ntrs.nasa.gov/api/citations/20050205045/downloads/20050205045.pdf

Sang H. Choi, H. J. K., and Robert W. M. (2023). "Electrostatic Power from Negatively Charged Lunar Regolith." *Journal of Aerospace Engineering and Mechanics* 7 (1): 621–35. https://doi.org/10.36959/422/468.

Symposium on Lunar Bases. (1988). *Symposium on Lunar Bases and Space Activities in the 21st Century,* Symposium Paper No. LBS-88-251. https://www.lpi.usra.edu/lpi/contribution_docs/LPI-000652.pdf

The European Space Agency. (2021). *Powering the Future with Lunar Soil*. https://www.esa.int/Enabling_Support/Preparing_for_the_Future/Discovery_and_Preparation/Powering_the_future_with_lunar_soil

Utilities One. (2023). *Engineering Challenges in Lunar Exploration: A Path to Discovery*. https://utilitiesone.com/engineering-challenges-in-lunar-exploration-a-path-to-discovery

Williams, D. R. (2020). Moon Fact Sheet. *NASA Goddard Space Flight Center*. https://nssdc.gsfc.nasa.gov/planetary/factsheet/moonfact.html.

Zhang, P., Dai, W., Niu, R., Zhang, G., Liu, G., Liu, X., and Bo, Z., et al. (2023). "Overview of the Lunar In Situ Resource Utilization Techniques for Future Lunar Missions." *Space: Science and Technology (United States)* 3: 1–18. https://doi.org/10.34133/s